Influence of air preheat temperature and excess air in a reverse flow combustor

Djamel Benmenine[1,2,*], Abdelhalim Bentebbiceh[1]

1. Laboratoire de Mécanique Énergétique et Systèmes de Conversion, Université des Sciences et de Technologie Houari Boumédiène BP32, El-Alia, 16111 Bab-Ezzouar, Alger, Algeria

2. Laboratoire de développement des énergies nouvelles et renouvelables en zones arides (LENREZA), Université Kasdi Merbah Ouargla BP 511, 30000 Ouargla, Algeria

benmenine.djamel@tecnico.ulisboa.pt

ABSTRACT. *The purpose of this study is to investigate The influence of the air preheat temperature and excess air coefficient on the combustion process. For that, Combustion in a stagnation point reverse flow small-scale cylindrical combustor is numerically simulated. The burner and the exhaust port are located at the top of the combustor and the bottom end is closed. The fuel is natural gas. Turbulence is modelled using either the Reynolds stress model or large eddy simulation (LES). In the former case, two different combustion models are used, namely the eddy dissipation finite rate (ED-FR) model with a two-step reaction mechanism, and the eddy dissipation concept (EDC) along with a detailed reaction mechanism. In the case of LES, only the ED-FR model is employed.. Through this study, it was found that The temperature field becomes more uniform when the excess air coefficient or the air preheat temperature increase. If the excess air coefficient increases, the maximum and average temperatures in the combustor are lower, as well as the heat release rate, the scalar gradients are smoother, the reaction zone becomes wider, and moves away from the burner. The increase of the preheat air temperature yields an increase of the maximum and averaged temperatures in the combustor, and an increase of the heat release rate, with a thinner and shorter reaction zone that is closer to the burner. Satisfactory predictions of the NO emissions were obtained.*

RÉSUMÉ. *Le but de cette étude est d'étudier l'influence de la température de préchauffage de l'air et du coefficient d'air en excès sur le processus de combustion. À cette fin, des simulations numériques de la combustion dans la petite chambre de combustion cylindrique à contre-courant au point de stagnation sont simulées numériquement. Le brûleur et l'orifice d'échappement sont situés dans la partie supérieure de la chambre de combustion et le bas est fermé. Le carburant est du gaz naturel. La turbulence est modélisée à l'aide du modèle de stress de Reynolds ou de la simulation par grands tourbillons (LES). Dans le premier cas, deux modèles de combustion différents ont été utilisés, à savoir le modèle de dissipation à vitesse limitée par tourbillon (ED-FR) avec un mécanisme de réaction en deux étapes, et le concept de dissipation de tourbillon (EDC) avec un mécanisme de réaction détaillé. Dans le*

cas des LES, seul le modèle ED-FR a été utilisé. Cette étude a révélé que le champ de température devient plus uniforme lorsque le coefficient d'air en excès ou la température de préchauffage de l'air augmentent. Si le coefficient d'excès d'air augmente, les températures maximales et moyennes dans la chambre de combustion sont plus basses, ainsi que le taux de dégagement de chaleur, les gradients scalaires sont plus lisses, la zone de réaction devient plus large et s'éloigne du brûleur. L'augmentation de la température de l'air de préchauffage entraîne une augmentation des températures maximales et moyennes dans la chambre de combustion et une augmentation du taux de dégagement de chaleur, avec une zone réactionnelle plus fine et plus courte, plus proche de la chambre de combustion. Des prévisions satisfaisantes des émissions de NO ont été obtenues.

KEYWORDS: *reverse-flow combustor, eddy dissipation concept, air-preheat temperature, excess air.*

MOTS-CLÉS: *chambre de combustion à flux inverse, concept de dissipation de tourbillon, température de préchauffage de l'air, excès d'air.*

DOI:10.3166/I2M.17.93-111 © 2018 Lavoisier

1. Introduction

The need to burn fuels efficiently with low pollutant emissions has been the concern of combustion engineers for many years. Different technologies have been developed for that purpose, namely lean premixed combustion, exhaust gas recirculation, water or steam injection, catalytic combustion and mild combustion. Another possibility is the use of novel combustor geometries, such as the reverse flow combustor. These combustors have been widely studied and used in gas turbine engines, e.g., Bharani *et al.* (2001). since they present several advantages, such as the reduction of the length of the gas turbine. A more recent configuration is the stagnation point reverse flow combustor

In stagnation point reverse flow combustors, the burner and the exhaust are both placed at the same side of the combustor, while the opposite side is closed. Several authors studied these combustors operating in the conventional combustion regime, e.g., Mansour *et al.* (1989). or with very lean fuel-air mixtures (Gopalakrishnan *et al.,* 2007; Bobba *et al.,* 2008; Undapalli *et al.,* 2009). Experimental studies in a stagnation point reverse flow combustor operating in the mild combustion regime were originally performed by Plessing *et al.* (1998) and Özdemir and Peters (2001), while numerical simulations were reported by Coelho and Peters (2001) and Dally *et al.* (2004). A reverse flow combustor with square cross-section was designed and experimentally studied by Szegö *et al.* (2008; 2009). Duwig and Iudiciani (2014) reported LES results computed using the thickened flame model and detailed chemistry for the combustor experimentally investigated by Undapalli *et al.* (2009). More recently, Kruse *et al.* (2015) studied the influence of pressure on the mild combustion process and on emissions in a combustor similar to that used by Plessing *et al.* (1998).

The present work is concerned with the numerical simulation of the stagnation point reverse flow in the cylindrical combustor experimentally studied by Castela *et al.* (2012). Detailed temperatures and species concentration measured inside the

combustor are available for three different operating conditions. Simulations for two of these cases were reported by Graça *et al.* (2013) using Ansys-Fluent. Predictions based on the eddy dissipation concept and on the composition PDF method revealed a good agreement with the experimental data, except in the region downstream of the burner and in the vicinity of the centerline, up to about one-half of the combustor length, where the predicted temperatures and oxygen molar fraction are lower than the measured ones, while the CO_2 molar fraction is overestimated reported by Lamouroux *et al.* (2014). Lamouroux *et al.* (2014) assumed a non-premixed flame structure and performed LES calculations using a detailed chemistry tabulation procedure that extends the flame let/progress variable formulation by including information on the intensity of internal dilution and heat loss. This model yielded reasonably good predictions of the temperature, O_2 and CO_2 molar fractions along the centerline for an excess air coefficient of 2.4 and air preheat temperature of 600 K. Nevertheless, discrepancies were still observed in the region close to the nozzle. Liu and Zheng (2013) used the standard k-ε model and the eddy dissipation concept (EDC) to investigate the influence of air inlet conditions. They claim good results for the same operating conditions studied by Lamouroux *et al.* (2014). when the time scale and volume fraction constants of the EDC model were tuned, in contrast with the predictions of Graça *et al.* (2013), which were only moderately improved by changing those constants

The experiments of Castela *et al.* (2012) include detailed experimental data for three different operating conditions, and flue gas composition and hydroxyl radical chemiluminescence (OH*) images for several values of inlet air preheat temperatures and excess air coefficients. A few of these operating conditions correspond to mild combustion, while others do not. Numerical simulations for this range of conditions were not previously performed. The present work reports LES predictions carried out using the ED-FR model, which are compared with results obtained using the Reynolds stress model for turbulence closure along with the ED-FR and the EDC models for combustion. The predictions are assessed using experimental data from Castela *et al.* (2012). In addition, the influence of the air preheat temperature and excess air coefficient is numerically investigated, and predictions of NO emissions are compared with the measurements. The purpose of this study is to find out to what extent currently available commercial software is able to reproduce the experimental data and the observed trends when the operating conditions are changed. Hence, the present results provide an insight on the predictive ability of models available in commercial codes for different combustion regimes in a small scale stagnation point reverse flow combustor.

2. Mathematical modelling

The mathematical model is based on the solution of the governing equations for mass, momentum and energy, and on transport equations for the turbulence and combustion models. Two different methods were used in the present simulations for turbulence closure. In one of them, the Favre-averaged Navier-Stokes equations were solved and turbulence was modelled using the Reynolds stress model, which

requires the solution of transport equations for the turbulent stresses and for the dissipation rate of turbulent kinetic energy. In the other approach, LES was used, and the Favre-filtered governing equations were solved using the Smagorinsky-Lilly model (Smagorinsky, 1983) to calculate the sub grid-scale turbulent viscosity.

Combustion was simulated using either the ED-FR model (Magnussen and Hjertager, 1977) or the EDC model (Magnussen, 1981). In the former, the reaction rate of a species is taken as the minimum between the mixing and the kinetics rates. The EDC is an improved version of the eddy dissipation model, allowing for detailed finite-rate chemical kinetics in the simulation of turbulent reactive flows. The transport equations for the species are solved during the CFD calculations. The EDC model relies on the Kolmogorov cascade of energy dissipation on all length scales in turbulent flows from the largest to the smallest eddies. The turbulent kinetic energy is converted into heat by viscous dissipation. The model assumes that chemical reactions and molecular mixing associated with turbulence dissipation occur within the fine structures of the flow. These fine structures are a small fraction of the total fluid volume, where the reactants are homogeneously mixed, as in a well stirred reactor. The mass fraction occupied by the fine structure regions is expressed as a function of the turbulent kinetic energy, its dissipation rate and the kinematic viscosity. The reactions occur in the fine structures over a residence time scale. The mean reaction rate of a species is inversely proportional to that time scale

The ED-FR model was used along with a two-step reaction scheme, while the EDC was employed with the DRM-19 chemical mechanism, which comprises 19 chemical species and 84 chemical reactions. This is a reduced version of the GRI-1.2 full mechanism, and was developed to obtain the smallest set of reactions needed to closely reproduce the main combustion characteristics predicted by the full mechanism. It was formerly found, for a similar combustor, that the predictions obtained using the DRM-19 and the GRI-1.2 mechanisms were very close to each other (Rebola *et al*., 2013). The GRI-1.2 is similar to the GRI-2.11mechanism, but does not include the nitrogen chemistry. Moreover, it was reported that the GRI-3.0 mechanism, which is the latest release of GRI-Mech and replaces the previous ones, does not perform as well as the GRI-2.11 mechanism for mild conditions (Fortunato *et al*., 2015). Hence, the DRM-19 constitutes a good compromise between computational requirements and expected accuracy of the chemical mechanism.

Thermal radiation was calculated using the discrete ordinates method. The radiative properties of the participating medium were modelled using the weighted-sum-of-grey gases model.

When the chemical mechanism includes the nitrogen chemistry, the prediction of NO concentration may be carried out using the EDC model, e.g. Fortunato *et al.* (2015). Otherwise, the calculation of NO molar fraction may be predicted in a post-processing stage by solving a transport equation for NO mass fraction and using simplified models for the different NO mechanisms, e.g. Galletti *et al.* (2007), Rebola *et al.* (2013). The thermal, prompt and N_2O mechanisms were considered in the present work. The NNH mechanism was found to be important in fuels containing nitrogen (Mardani and Tabejamaat, 2012) and a few authors pointed out

that the NO reburning mechanism also plays a role (Nicolle *et al*., 2006; Li *et al*., 2013), but these routes were not considered in the present work.

The thermal NO formation was predicted using the extended Zeldovich mechanism, along with a quasi-steady-state assumption for the concentration of the nitrogen atom. The instantaneous concentrations of the oxygen and hydroxyl atoms were evaluated from the EDC model.

The prompt NO formation was computed according to De Soete (1975). The formation of NO from molecular nitrogen via N_2O was considered by using a quasi-steady approximation. The mean reaction rates of NO were evaluated by integrating the instantaneous rate weighted by the pdf of the temperature and species, so that turbulent fluctuations are taken into account. The variance of temperature is estimated using an approximate algebraic expression derived from its transport equation by setting the production term equal to the dissipation term. An assumed clipped Gaussian pdf shape was used.

It is worth to point out that there are several options in the NO models available in Ansys-Fluent (e.g., calculation method of the O and OH concentrations, quasi-steady vs. solution of transport equation for N_2O, the pdf shape, calculation method for the variance of the temperature) that have a non-negligible effect on the NO prediction. The options used in this work were selected to improve the agreement with the experimental data for the calculations presented below.

3. Reverse flow combustor

The stagnation point reverse flow combustor schematically represented in Figure 1 was studied in the present work. The combustion chamber is cylindrical and vertically oriented, with an inner diameter of 100 mm and a length of 340 mm. The burner and the exhaust port are located at the top section of the combustion chamber, while the bottom section is closed by a stainless steel plate with a moving hole for the introduction of probes. The combustor operates at atmospheric pressure and the fuel thermal input is 8 kW. The fuel is supplied through a central tube with an inner diameter of 4 mm, and the inlet velocity is 17.7 m/s. Air is introduced through a concentric annular tube with inner and outer diameters of 14 mm and 18.5 mm, respectively. The combustion products exit the combustor chamber through an annular concentric orifice with inner and outer diameters of 75 mm and 90 mm, respectively. The combustion air may be preheated using an electrical heating system, and the fuel inlet temperature is 300 K. The air preheat temperature and the excess air coefficient for the cases studied in the present work are given in Table 1. The fuel is natural gas with the following volumetric composition: CH_4: 83.7%, C_2H_6: 7.6%, C_3H_8: 1.9%, N_2: 5.4%, other minor components: 1.4%.

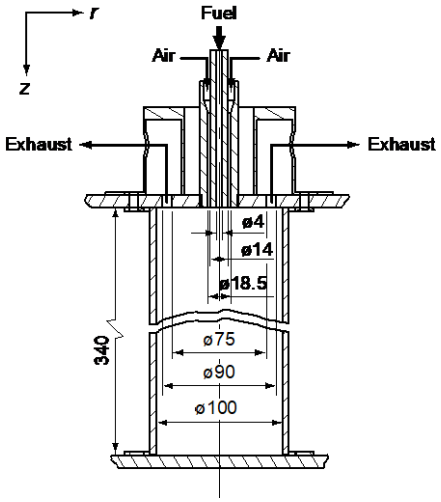

Figure 1. Schematic of the combustor

Measurements of the local mean temperature and O_2, CO_2, CO, UHC (unburnt hydrocarbons) and NO_x concentrations along several radial profiles were obtained for cases 2, 3 and 5 in Table 1, and the flue-gas chemical composition was measured for all conditions listed in that table. The temperature was measured using fine wire platinum/platinum:13% rhodium (type R) thermocouples, and the species concentrations were measured using a stainless steel water-cooled probe. In addition, OH* images for the entire combustion chamber were collected using an intensified charge-coupled device (ICCD) camera. Details of the experimental methods are presented in Castela *et al.* (2012), along with the report and discussion of the experimental data.

4. Computational details

The calculations were performed using three different methods, depending on the turbulence and combustion models employed: (i) Reynolds stress and ED-FR models; (ii) Reynolds stress and EDC models; (iii) LES and ED-FR models. Preliminary calculations for case (ii) were performed using two different 2D axisymmetric non-uniform structured meshes with approximately 14,000 and 50,000 control volumes. The inlet fuel and air ducts were included in the computational domain, in order to allow the flow to develop and to reduce the uncertainty in the values of the turbulent kinetic energy and dissipation rate at the combustor inlet. The results showed that the difference between the predictions for the two meshes was marginal (Graça *et al*., 2013). According to this analysis, the results presented below for methods (i) and (ii) were obtained for the coarsest mesh.

Uniform axial velocity profiles of air and fuel were prescribed at the inlet section of the air and fuel nozzles. The turbulent kinetic energy and the dissipation rate at the inlet were estimated following standard practices. Standard wall functions were used for the velocity boundary conditions at the walls of the combustor. The wall temperature was set to 1300 K. The emissivity of the solid boundaries was prescribed as 0.9. A pressure outlet boundary condition with zero gauge pressure was prescribed at the exhaust.

The calculations were performed using the Ansys-Fluent commercial software. All the governing equations for methods (i) and (ii) were solved using a second order upwind discretization scheme, and the SIMPLEC algorithm. The convergence criterion required that the sum of the residuals of the discretized equations over the domain decreased below 10^{-3}, except for the energy conservation equation, where a residual of 10^{-6} was considered. It was further checked that the values of the mean temperature and mass fractions of major species at several monitoring points of the computational domain become approximately constant during the iterative solution process.

The calculations for method (iii) were performed using a 3D mesh with about 4 million control volumes. The second-order upwind scheme was employed again, and the time discretization was carried out using a second-order implicit scheme, and a time step of 3×10^{-6}.

5. Results and discussion

Table 1. Test case

Case	Preheat air Temperature (K)	Excess air coefficient (λ)	Predicted maximum temperature (K)	Predicted average temperature (K)	T^*_{max}	K_v	NO_x in flue gas (ppm@15%O_2)	
							Experiments	Predictions
1	600	1.3	1930	1767	0.092	0.59	35	51.4
2	600	1.5	1780	1667	0.068	0.63	23	24.4
3	600	1.6	1740	1650	0.055	0.64	19	21.4
4	600	2.0	1580	1511	0.046	0.73	9	9.6
5	600	2.4	1480	1412	0.048	0.79	1	2.9
6	300	2.0	1412	1251	0.129	0.44	4	0.8
7	500	2.0	1525	1452	0.050	0.65	8	6.0
8	700	2.0	1627	1560	0.043	0.81	21	15.0
9	800	2.0	1682	1622	0.037	0.86	28	23.5

Predictions of the mean temperature and O_2, CO_2 and CO molar fractions were presented in Graça *et al* (2013) and compared with the experimental data of Castela *et al*. (2012). for cases 2 and 5 (see Table 1).

Those calculations were performed using the above mentioned mesh with approximately 14,000 control volumes. The *k-ε* and the EDC models were used along with the DRM19 chemical mechanism. Comparison of the predicted results with those computed using a finer mesh revealed negligible differences. The same mesh was used in the present work, along with the three different methods mentioned in the previous section.

5.1. Temperature and species concentration fields

Figure 2 shows predicted and measured radial profiles of the mean temperature and O_2, CO_2 and CO molar fractions at four different axial stations for case 2. The temperature close to the centerline is high at the two upstream stations (z=70 mm and z=150 mm), as well as the CO_2 molar fraction. Moreover, O_2 is consumed while CO_2 is formed from the first to the second station, and the O_2 and CO_2 molar fractions measured at *z*=150 mm do not change further downstream. This means that combustion occurs in this upstream region, and is completed at *z*=150 mm.

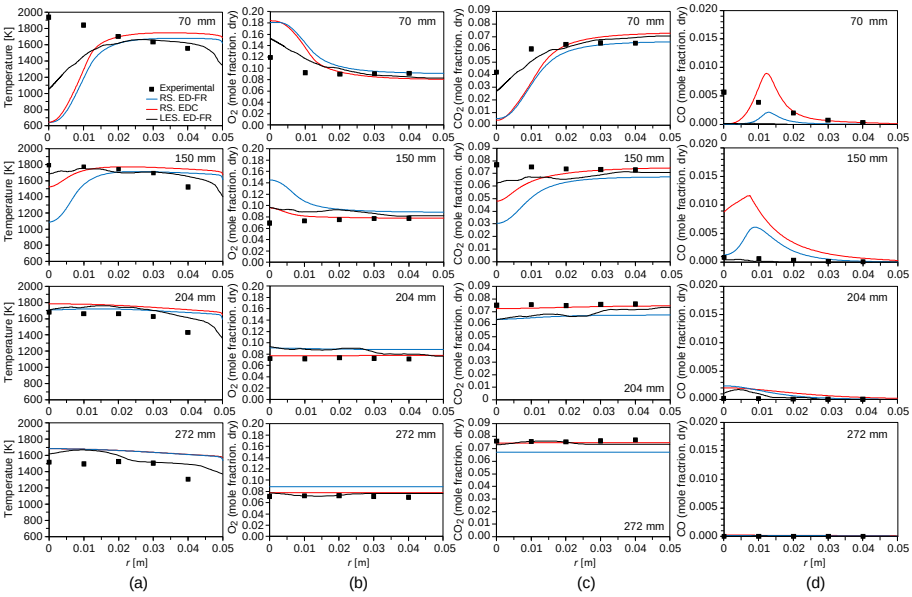

Figure 2. Radial profiles of predicted mean temperature, O_2, CO_2 and CO dry molar fractions for case 2

At z=70 mm, and in the vicinity of the centerline, the temperature is severely underpredicted, no matter the method employed. This is consistent with the excess of oxygen and the shortage of CO_2 and CO computed in that region. Despite the observed discrepancies, the LES model performs better than the others, as far as the temperature, O_2 and CO_2 molar fractions are concerned, but the predicted CO molar fraction is too low. The discrepancies observed at z=70 mm is also visible at z=150 mm, although the underprediction of temperature is smaller. Further downstream, the predictions are closer to the experiments.

A comparison between the results obtained using the two different combustion models along with the Reynolds stress model (methods 1 and 2) reveals significant differences between them. While the two models yield relatively similar results for the mean temperature and major species at z=70 mm, the EDC model clearly outperforms the ED-FR at z=150 mm. At the two last stations, although the computed temperature is somewhat high, the O_2 and CO_2 molar fractions calculated using the EDC closely match the experimental data. Overall, the EDC model, which involves a more detailed reaction mechanism, yields improved predictions in comparison with the ED-FR, as expected, except in the calculation of the CO molar fraction.

Clear differences are also found when the results calculated using the Reynolds stress model and LES, along with the ED-FR model (methods 1 and 3), are compared between them. The results predicted using Reynolds stress and ED-FR models (method 1) are the least accurate ones. Therefore, the LES model performs consistently better than the Reynolds stress model, and the EDC is more accurate than the ED-FR. Hence, calculations carried out using LES and EDC are expected to provide the best results. Still, these would require a major increase in computational time. This is only feasible using a parallel cluster, which is not affordable for most practical applications at present. Method 2 (Reynolds stress and EDC models) was used to perform the parametric study presented in the remainder of this article.

5.2. Influence of the excess air coefficient

The excess air coefficient was varied by changing the air mass flow rate, and therefore the air inlet velocity and momentum, while keeping the fuel mass flow rate fixed. The air preheat temperature was maintained constant and equal to 600 K. The influence of the excess air coefficient, λ, on the recirculation rate is shown in Table 1. The recirculation rate, defined by Wünning and Wünning (1997) as the ratio of the mass flow rate of recirculated exhaust gases to the mass flow rate of reactants, was computed following the procedure described by Rebola *et al.* (2013). The calculated recirculation rate, kv, increases slightly with the excess air coefficient, as shown in Table 1. The computed values are slightly lower than those reported by Liu and Zheng (2013). for cases 2, 4 and 5, which were 0.71, 0.83 and 0.91, respectively, and Graça *et al*. (2013) for case 4, which was 1.0. All these values are far below the limit of 3 above which flameless combustion takes place, according to Wünning and Wünning (1997).

The influence of the excess air coefficient on the predicted mean temperature, O_2 and CO_2 molar fractions, on a dry basis, is illustrated in Figure 3. The model predicts a relatively low temperature in a region downstream of the burner and in the vicinity of the centerline, where the concentration of oxygen is high, and the concentration of CO_2 is low. In the case of $\lambda<2$, that region is surrounded by a narrow layer of high temperature and species concentration gradients, typical of a conventional diffusion flame, where combustion is taking place and heat release rate is highest. These gradients are attenuated for $\lambda\geq2$. On the outer side of this layer, the concentration of CO_2 remains relatively high over the combustor, as a consequence of the internal recirculation of combustion products. The length of the layer increases and the maximum temperature along the centerline is reached further downstream when the excess air increases.

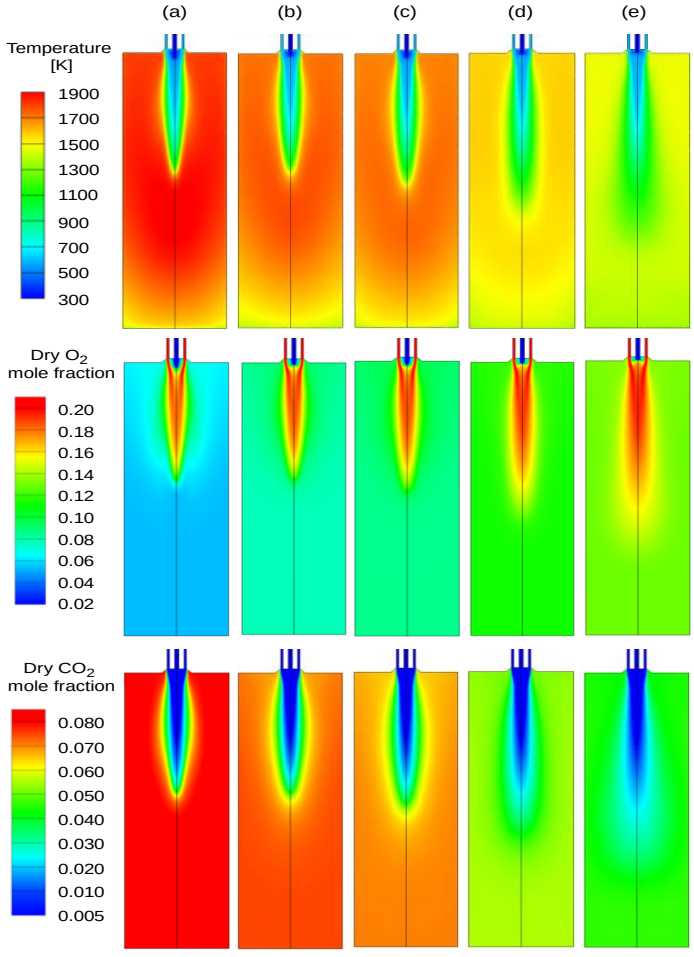

Figure 3. Predicted mean temperature field for cases 1 to 5. (a) λ =1.3, (b) λ =1.5, (c) v=1.6, (d) λ =2.0, (e) λ=2.4

The volumetric heat release rate is shown in Figure 4. It is defined as minus the sum, extended over all chemical species, of the product of the standard enthalpy of formation by the reaction rate of the species. The layer of large gradients of temperature and species concentration is coincident with the zone where the heat release rate is highest. This layer is thinner and the volumetric heat release rate is higher for lower values of λ. The heat release rate decreases and the reaction zone spreads over a larger volume when the excess air coefficient increases.

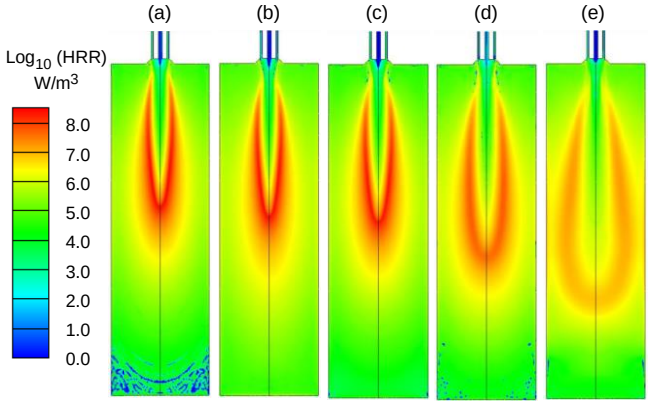

Figure 4. Predicted heat release rate for cases 1 to 5. (a) λ =1.3, (b) λ =1.5, (c) v=1.6, (d) λ =2.0, (e) λ=2.4

Both the maximum and the average temperatures in the combustor decrease with the increase of the excess air coefficient, as expected (see Table 1). The computed temperatures downstream of the burner are relatively low, but they remain approximately uniform elsewhere. The temperature uniformity may be quantified using the normalized temperature deviation, T*, defined as follows:

$$T^* = \frac{T - \overline{T}}{\overline{T}} \tag{1}$$

where T is the local mean temperature and $\overline{T}$ is the volume weighted average of the mean temperature. The contours of the normalized temperature deviation are displayed in Figure 5. The values of T* are slightly higher when the excess air is lower, and decrease with the increase of the excess air coefficient. Therefore, the increase of the excess air coefficient promotes the uniformity of the temperature field.

The predicted values of T* for T=Tmax, denoted as T^*_{max}, are given in Table 1. These values are consistent with those predicted by Liu and Zheng (2013) for cases 2, 4 and 5, which were 0.080, 0.049 and 0.037, respectively.

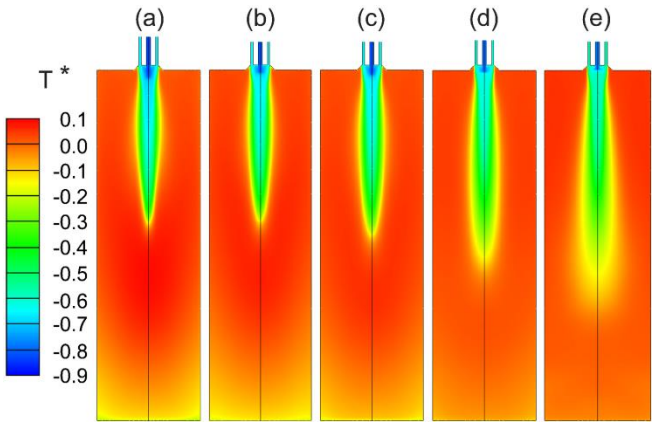

Figure 5. Contours of the normalized temperature deviation for cases 1 to 5 (a) λ=1.3, (b) λ=1.5, (c) v=1.6, (d) λ=2.0, (e) λ=2.4

The electronically excited hydroxyl radical, OH*, provides information on the position and size of the reaction zone in combustion systems (Böhm *et al*., 2013). Hence, contours of the OH* concentration are expected to be qualitatively similar to those of the volumetric heat release rate. Mean OH* chemiluminescence images were reported by Castela *et al.* (2012). The experiments reveal that the OH*intensity is highest for λ =1.3, and the OH* gradients are largest in this case. As the excess air coefficient increases, the OH* intensity decreases, its gradients become smaller, and the region where the concentration is highest moves towards the bottom of the combustor. These features are consistent with the predicted temperature field and the heat release rate, i.e., the mean temperature and the heat release rate decrease and become more uniform when the OH*intensity decreases. However, the region of maximum OH* intensity in the experimental image resembles two neighboring ellipses, while the region where the predicted heat release rate is highest looks like an elliptical annulus that was cut at the side close to the burner. Moreover, the region of highest OH* intensity in the experiments is closer to the burner, in comparison with the predictions. These differences are related to the underprediction of temperature along the axis, downstream of the burner, which can be seen in Figure 2.

The OH* images reported by Castela *et al*. (2012) for the lowest values of the excess air coefficient show a well-defined reaction zone. Moreover, the measured temperatures were relatively high, as well as the gradients of species concentrations (see, e.g., Figure 2 for v=1.5), and therefore a conventional lean combustion regime occurs for these conditions. When the excess air increases, in particular for $\lambda \geq 2$, Castela *et al*. (2012) observed that the luminosity of the flame decreased, no matter the air preheat temperature. It is well known that the temperature field is relatively uniform in mild combustion. Hence, given the lower values of T* and the lower OH* intensity for higher values of the excess air coefficient, mild conditions are

expected to prevail in the combustor chamber in that case. Therefore, it can be concluded that the combustion regime gradually changes from conventional combustion, when the excess air is smaller, to mild combustion for higher excess air. It is worth to point out that a different trend was reported by Veríssimo *et al.* (2011), but it should be realized that their study was performed in a different combustor, in which the burner and the exhaust were located at opposite sides of the combustion chamber.

In Table 1, the predicted NO emissions are compared with the experimental data for the NOx emissions, corrected to 15% O2 at the exhaust. The predicted NO emissions are almost exclusively due to the N2O mechanism. In case 4, for example, this mechanism is responsible for more than 90% of the emissions. The predictions are quite satisfactory, regarding the simplicity of the model employed, except for case 1, where the emissions were overestimated by more than 40%. The decrease of the NO emissions with the increase of the excess air coefficient is correctly predicted by the model. This trend, which was also reported by Galletti *et al.* (2007) and Arghode *et al.* (2012), may be explained by two different effects. First, as the excess air increases, so does the recirculation rate, and therefore more products are transported to the reaction zone, lowering the temperature and decreasing the molar fraction of oxygen. Second, the residence times are lower due to the increase of the inlet air velocity.

5.3. Influence of the air preheat temperature

The influence of the inlet air temperature, Tin, on the recirculation rate is shown in Table 1. The excess air coefficient was maintained constant and equal to 2. Therefore, the inlet air velocity increases with the inlet air temperature, since the air mass flow rate does not change, but the density decreases. The recirculation rate increases continuously with the air preheat temperature due to the increase of the inlet air velocity, for a fixed air mass flow rate, which entrains more recirculated combustion products. This behavior is consistent with the findings of Mosca *et al.* (2013).

Figure 6 shows the influence of the air preheat temperature on the predicted mean temperature, O_2 and CO_2 molar fractions. The temperatures in the combustor increase with the increase of the preheat air temperature, while the layer of strong scalar gradients becomes shorter and thinner. The O_2 and CO_2 concentrations are consistent with those trends. The volumetric heat release rate contours displayed in Fig. 7 further demonstrate that the reaction rate is lower and extends over a wider region when the air is not preheated. The heat release rate increases, and the reaction zone exhibits sharper gradients and moves upstream with the increase of the air preheat temperature.

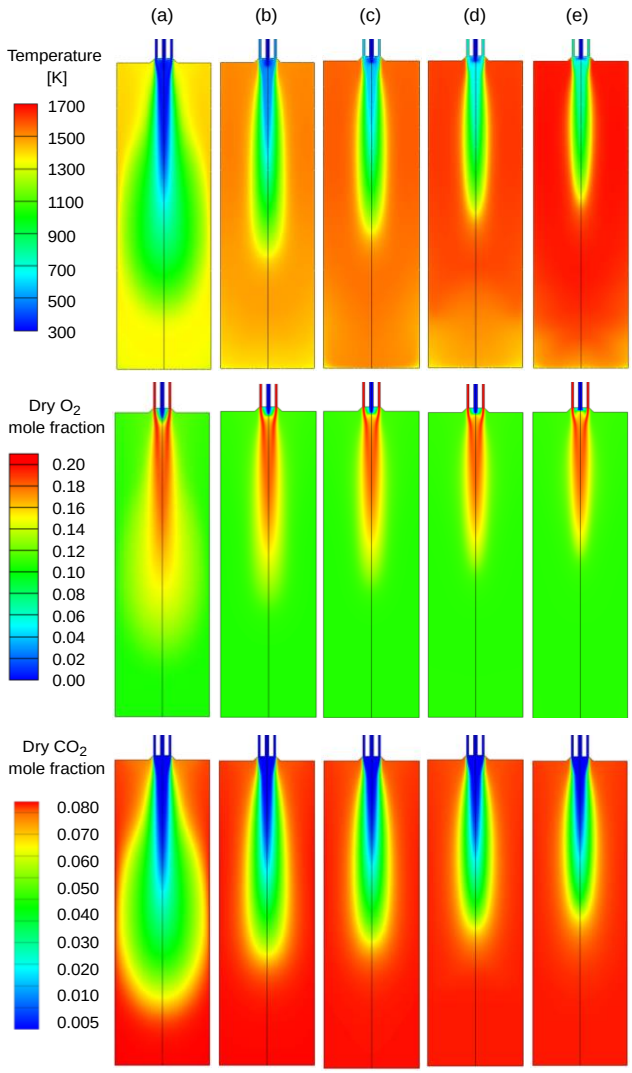

Figure 6. Predicted mean temperature field for cases 6 to 9. (a) T_{in}=300 K, (b) T_{in}=500 K, (c) T_{in}=600 K, (d) T_{in}=700 K, (e) T_{in}=800 K

The maximum and the average temperatures, given in Table 1, increase with the increase of the air preheat temperature, as expected, but the normalized temperature deviation decreases, as shown in Fig. 8, and as suggested by T^*_{max}. Therefore, the temperature field becomes more uniform when Tin is higher. This trend, which was formerly reported by Gupta (2004), is consistent with the experiments by Veríssimo *et al.* (2015), even though these were carried out in a different combustor.

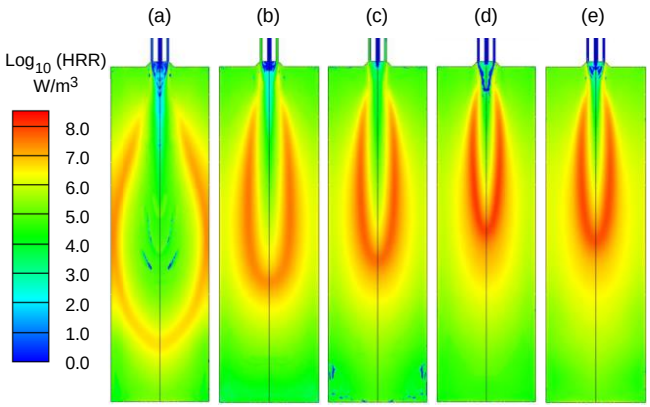

Figure 7. Predicted heat release rate (HRR) for cases 6 to 9. (a) T_{in}=300 K, (b) T_{in}=500 K, (c) T_{in}=600 K, (d) T_{in}=700 K, (e) T_{in}=800 K

The mean OH* chemiluminescence images presented in Castela *et al.* (2012) show that the OH*intensity increases with the increase of the air preheat temperature, in agreement with the observations of Mosca *et al.* (2013), because the temperatures in the combustor become higher, while the region where the maximum values are achieved shifts towards the burner. This shift is due to the reduction of the ignition delay time when Tin increases, so that chemical reactions take place closer to the burner. The predictions corroborate these observations. However, the predicted contours of the volumetric heat release rate and the OH* images differ on the shape of the region of highest values/intensities and on the distance from the burner to that region, as also observed in section 5.2, when the excess air coefficient varied.

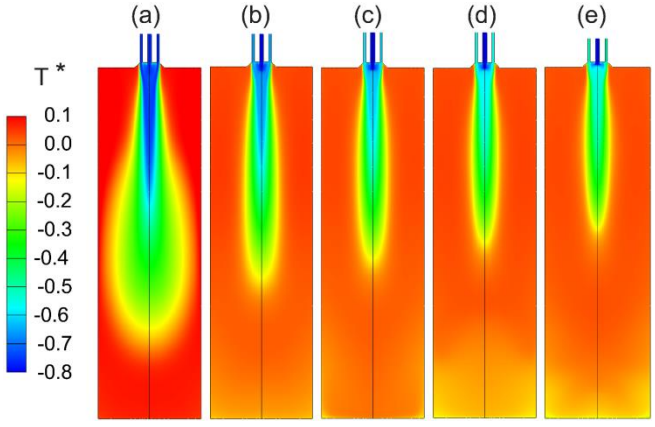

Figure 8. Contours of the normalized temperature deviation for cases 6 to 9.(a) T_{in}=300 K, (b) T_{in}=500 K, (c) T_{in}=600 K, (d) T_{in}=700 K, (e) T_{in}=800 K

The predicted NO emissions, corrected to 15% O_2 at the exhaust, are in very satisfactory agreement with the experimental results, as shown in Table 1. The NO emissions increase with the increase of the air preheat temperature. A similar trend was reported by Dally *et al*. (2004), Gupta (2004) and Mosca *et al*. (2013). However, the maximum mean temperatures are relatively low, anticipating that the thermal NO mechanism is not relevant for these operating conditions, since this NO formation mechanism is only important for temperatures above 1800 K. Even though turbulent fluctuations may cause instantaneous temperatures greater than that, the N_2O path mechanism was found to be by far the most important one for the studied cases.

6. Conclusions

A stagnation point reverse flow combustor was numerically simulated using three different methods: (1) Reynolds stress model, ED-FR and a two-step reaction mechanism; (2) Reynolds stress model, EDC and DRM19 reaction mechanism; (3) LES, ED-FR and a two-step reaction mechanism. The performance of these methods was investigated for an excess air coefficient of 1.5 and a preheat air temperature of 600 K. Then, eight additional operating conditions, with different excess air coefficients and air preheat temperatures, were investigated using method (2). The following conclusions may be drawn from the analysis carried out:

(1) The recirculation rate increases slightly with the increase of the excess air coefficient and with the increase of the preheat air temperature.

(2) The increase of the excess air coefficient promotes the uniformity of the temperature field, and yields a decrease of the maximum and average temperatures.

(3) If the excess air coefficient increases, the predicted heat release rate decreases, as well as its gradients. Moreover, the region where the heat release rate is highest becomes wider and moves away from the burner, while the gradients are smoother. These trends are corroborated by the experimental hydroxyl radical chemiluminescence OH* images.

(4) The increase of the air preheat temperature also enhances the uniformity of the temperature field, but the maximum and average temperatures become higher.

(5) If the air preheat temperature increases, the predicted heat release rate increases as well, and the region where its gradients are highest is thinner, shorter, and moves towards the burner.

(6) Predictions of the NO emissions are in fair to good agreement with the measurements. They increase when the excess air coefficient is reduced or the air preheat temperature increases. The N_2O mechanism is by far the most important one in the formation of NO for the considered operating conditions.

Acknowledgements

This work was supported by: FCT, through IDMEC, under LAETA, project UID/EMS/50022/2013 and Ministry of Higher Education and Scientific Research in Algeria

References

Arghode V. K., Gupta A. K., Bryden K. M. (2012). High intensity colorless distributed combustion for ultra low emissions and enhanced performance. *Applied Energy*, Vol. 92, pp. 822-830. http://dx.doi.org/10.1016/j.apenergy.2011.08.039

Bharani S., Singh S. N., Agrawal D. P. (2001). Effect of swirl on the flow characteristics in the outer annulus of a prototype reverse-flow gas turbine combustor. *Experimental Thermal and Fluid Science*, Vol. 25, pp. 337-347. http://dx.doi.org/10.1016/S0894-1777(01)00089-9

Bobba M. K., Gopalakrishnan P., Periagaram K., Seitzman J. M. (2008). Flame structure and stabilization mechanisms in a stagnation point reverse flow combustor. *Journal of Engineering for Gas Turbines and Power*, Vol. 130, No. 1, pp. 879-888. http://dx.doi.org/10.1115/GT2007-28231

Böhm B., Geyer D., Gregor M. A., Heeger C., Nauert A., Scneider C., Dreizler A. (2013). Advanced Laser diagnostics for understanding turbulent combustion and model validation. *Flow and Combustion in Advanced Gas Turbine Combustors*, Vol. 1581, pp. 93-160. https://doi.org/10.1007/978-94-007-5320-4_4

Castela M., Veríssimo A. S., Rocha A. M. A., Costa M. (2012). Experimental study of the combustion regimes occurring in a laboratory combustor. *Combust. Sci. Technol*, Vol. 184, No. 2, pp. 243-258. https://doi.org/10.1080/00102202.2011.630592

Coelho P. J., Peters N. (2001). Numerical simulation of a mild combustion burner. *Combustion & Flame*, Vol. 124, No. 3, pp. 503-518. https://doi.org/10.1016/S0010-2180(00)00206-6

Dally B. B., Riesmeier E., Peters N. (2004). Effect of fuel mixture on moderate and intense low oxygen dilution combustion. *Combustion and Flame*, Vol. 137, No. 3, pp. 418-431. https://doi.org/10.1016/j.combustflame.2004.02.011

De Soete G.G. (1975). Overall reaction rates of NO and N_2 formation from fuel nitrogen. *Proc. Combust. Inst*, Vol. 15, No. 1, pp. 1093-1102. https://doi.org/10.1016/S0082-0784(75)80374-2

Duwig C., Iudiciani P. (2014). Large Eddy Simulation of turbulent combustion in a stagnation point reverse flow combustor using detailed chemistry. *Fuel*, Vol. 123, pp. 256-273. https://doi.org/10.1016/j.fuel.2014.01.072

Fortunato V., Galletti C., Tognotti L., Parente A. (2015). Influence of modelling and scenario uncertainties on the numerical simulation of a semi-industrial flameless furnace. *Applied Thermal Engineering*, Vol. 76, pp. 324-334. https://doi.org/10.1016/j.applthermaleng.2014.11.005

Galletti C., Parente A., Tognotti L. (2007). Numerical and experimental investigation of a mild combustion burner. *Combustion and Flame*, Vol. 151, No. 3, pp. 649-664. https://doi.org/10.1016/j.combustflame.2007.07.016

Gopalakrishnan P., Bobba M. K., Seitzman J. M. (2007). Controlling mechanisms for low NOx emissions in a non-premixed stagnation point reverse flow combustor. *Proceedings of the Combustion Institute*, Vol. 31, No. 2, pp. 3401-3408. https://doi.org/10.1016/j.proci.2006.07.256

Graça M., Duarte A., Coelho P. J., Costa M. (2013). Numerical simulation of a reversed flow small-scale combustor. *Fuel Processing Technology*, Vol. 107, pp. 126-137. https://doi.org/10.1016/j.fuproc.2012.06.028

Gupta A. K. (2004). Thermal characteristics of gaseous fuel flames using high temperature air. *Journal of Engineering for Gas Turbines & Power*, Vol. 126, No. 1, pp. 9-19. https://doi.org/10.1115/1.1610009

Kruse S., Kerschgens B., Berger L., Varea E., Pitsch H. (2015). Experimental and numerical study of MILD combustion for gas turbine applications. *Applied Energy*, Vol. 148, pp. 456-465. https://doi.org/10.1016/j.apenergy.2015.03.054

Lamouroux J., Ihme M., Fiorina B., Gicquel O. (2014). Tabulated chemistry approach for diluted combustion regimes with internal recirculation and heat losses. *Combustion and Flame*, Vol. 161, No. 8, pp. 2120-2136. https://doi.org/10.1016/j.combustflame.2014.01.015

Li P., Dally B. B., Mi J., Wang F. (2013). MILD oxy-combustion of gaseous fuels in a laboratory-scale furnace. *Combustion and Flame*, Vol. 160, No. 5, pp. 933-946. https://doi.org/10.1016/j.combustflame.2013.01.024

Liu, X., Zheng, H. (2013). Numerical simulation of air inlet conditions influence on the establishment of MILD combustion in stagnation point reverse flow combustor. *Math. Problems Eng*. Article ID 593601.

Magnussen B. F. (1981). On the structure of turbulence and a generalized eddy dissipation concept for chemical reaction in turbulent flow. *19th AIAA Aerospace Science Meeting*, AIAA-2006-0962. https://doi.org/10.2514/6.1981-42

Magnussen B. F., Hjertager B. H. (1977). On mathematical modeling of turbulent combustion with special emphasis on soot formation and combustion. *Proc. Combust. Inst*, Vol. 16, No. 1, pp. 719-729. https://doi.org/10.1016/S0082-0784(77)80366-4

Mansour M. S., Bilger R. W., Dibble R. W. (1989). Raman/Rayleigh and Mie-scattering measurements in a reverse flow reactor close to extinction. *Proc. Combust. Inst*, Vol. 22, No. 1, pp. 711-719. http://dx.doi.org/10.1016/S0082-0784(89)80079-7

Mardani A., Tabejamaat S. (2012). NOx formation in H_2-CH_4 blended flame under mild conditions. *Combust. Sci. Technol,* Vol. 184, pp. 995-1010.

Mosca G., Lupant D. Gambale A., Lybaert P. (2013). Effect of air preheating temperature on flameless combustion of low calorific, alternative fuels. *Proc. European Combustion Meeting*, Lund, Sweden, 25-28 June.

Nicolle A., Dagaut P. (2006). Occurrence of NO-reburning in MILD combustion evidenced via chemical kinetic modeling. *Fuel*, Vol. 85, No. 17, pp. 2469-2478. http://dx.doi.org/10.1016/j.fuel.2006.05.021

Özdemir B. I., Peters N. (2001). Characteristics of the reaction zone in a combustor operating at mild combustion. *Experiments in Fluids*, Vol. 30, pp. 683-695. http://dx.doi.org/10.1007/s003480000248

Plessing T., Peters N., Wünning J. G. (1998). Laseroptical investigation of highly preheated combustion with strong exhaust gas recirculation. *Proc. Combust. Inst*, Vol. 27, pp. 3197-3204. http://dx.doi.org/10.1016/S0082-0784(98)80183-5

Rebola A., Coelho P. J., Costa M. (2013). Assessment of the performance of several turbulence and combustion models in the numerical simulation of a flameless combustor. *Combust. Sci. Technol*, Vol. 185, pp. 600-626. http://dx.doi.org/10.1080/00102202.2012.739222

Smagorinsky J. (1963). General circulation experiments with the primitive equations. *Monthly Weather Review*, Vol. 91, pp. 99-163.

Szegö G. G., Dally B. B., Nathan G. J. (2008). Scaling of NOx emissions from a laboratory-scale mild combustion furnace. Combust. Flame, Vol. 154, pp. 281-295. http://dx.doi.org/10.1016/j.combustflame.2008.02.001

Szegö G. G., Dally B. B., Nathan G. J. (2009). Operational characteristics of a parallel jet MILD combustion burner system. *Combust. Flame*, Vol. 156, pp. 429-438. http://dx.doi.org/10.1016/j.combustflame.2008.08.009

Undapalli S., Srinivasan S., Menon S. (2009). LES of premixed and non-premixed combustion in a stagnation point reverse flow combustor. *Proc Combust. Inst*, Vol. 32, No. 1, pp. 1537-1544.

Veríssimo A. S., Rocha A. M. A. Costa M. (2011). Operational, combustion and emission characteristics of a small-scale combustor. *Energy Fuels*, Vol. 25, pp. 2469-2480. http://dx.doi.org/10.1021/ef200258t

Veríssimo A. S., Rocha A. M. A., Coelho P. J., Costa M. (2015). Experimental and numerical investigation of the influence of the air preheating temperature on the performance of a small-scale mild combustor. *Combust. Sci. Technol*, Vol. 187, pp. 1724-1741. http://dx.doi.org/10.1080/00102202.2015.1059330

Wünning J. A., Wünning J. G. (1997). Flameless oxidation to reduce thermal NO-formation. *Prog. Energ. Combust. Sci*, Vol. 23, pp. 81-94. http://dx.doi.org/10.1016/S0360-1285(97)00006-3